THE PROTEIN SOCIETY

In silico and *in vitro* studies to elucidate the role of Cu^{2+} and galanthamine as the limiting step in the amyloid beta (1–42) fibrillation process

Maricarmen Hernández-Rodríguez,[1,2] José Correa-Basurto,[1]* Claudia G. Benitez-Cardoza,[3] Aldo Arturo Resendiz-Albor,[4] and Martha C. Rosales-Hernández[2]*

[1]Laboratorio de Modelado Molecular y Bioinformatica, Escuela Superior de Medicina, Instituto Politécnico Nacional, Plan de San Luis y Díaz Mirón s/n, 11340 México City, D.F., México

[2]Laboratorio de Biofísica y Biocatálisis, Escuela Superior de Medicina, Instituto Politécnico Nacional, Plan de San Luis y Díaz Mirón s/n, 11340 México City, D.F., México

[3]Laboratorio de Investigación Bioquímica. Laboratorio de Investigación Bioquímica, Sección de Estudios de Posgrado e Investigación. ENMyH-Instituto Politécnico Nacional, Guillermo Massieu Helguera No. 239, La Escalera Ticoman, 07320 México City, D.F., México

[4]Laboratorio de Investigación en Inmunología., Escuela Superior de Medicina, Instituto Politécnico Nacional, Plan de San Luis y Díaz Mirón s/n, 11340 México City, D.F., México

Received 8 April 2013; Revised 3 July 2013; Accepted 12 July 2013
DOI: 10.1002/pro.2319
Published online 31 July 2013 proteinscience.org

Abstract: The formation of fibrils and oligomers of amyloid beta (Aβ) with 42 amino acid residues ($A\beta_{1-42}$) is the most important pathophysiological event associated with Alzheimer's disease (AD). The formation of Aβ fibrils and oligomers requires a conformational change from an α-helix to a β-sheet conformation, which is encouraged by the formation of a salt bridge between Asp 23 or Glu 22 and Lys 28. Recently, Cu^{2+} and various drugs used for AD treatment, such as galanthamine (Reminyl®), have been reported to inhibit the formation of Aβ fibrils. However, the mechanism of this inhibition remains unclear. Therefore, the aim of this work was to explore how Cu^{2+} and galanthamine prevent the formation of $A\beta_{1-42}$ fibrils using molecular dynamics (MD) simulations (20 ns) and *in vitro* studies using fluorescence and circular dichroism (CD) spectroscopies. The MD simulations revealed that $A\beta_{1-42}$ acquires a characteristic U-shape before the α-helix to β-sheet conformational change. The formation of a salt bridge between Asp 23 and Lys 28 was also observed beginning at 5 ns. However, the MD simulations of $A\beta_{1-42}$ in the presence of Cu^{2+} or galanthamine demonstrated that both ligands prevent the formation of the salt bridge by either binding to Glu 22 and Asp 23 (Cu^{2+}) or to Lys 28 (galanthamine), which prevents $A\beta_{1-42}$ from adopting the U-characteristic conformation that allows the amino acids to transition to a β-sheet conformation. The docking results revealed that the conformation obtained by the MD simulation of a monomer from the 1Z0Q structure can form similar interactions to those obtained from the 2BGE structure in the oligomers. The *in vitro* studies demonstrated that Aβ remains in an unfolded conformation when Cu^{2+} and galanthamine are used. Then, ligands that bind Asp 23 or Glu 22 and Lys 28 could therefore be used to prevent β turn formation and, consequently, the formation of Aβ fibrils.

Grant sponsor: CONACYT; Grant numbers: 84119, 132353; Grant sponsors: ICyTDF, Pfizer, and COFAA-SIP/IPN; Grant numbers: 20110619/0786/1112/3893; 20121109/1242.

*Correspondence to: Jose Correa, Laboratorio de Modelado Molecular y Bioinformática, Sección de Estudios de Posgrado e Investigación, Escuela Superior de Medicina, Instituto Politécnico Nacional, Plan de San Luis y Díaz Mirón, 11340, México City, México. E-mail: corrjose@gmail.com or Martha C. Rosales-Hernández. E-mail: marcrh2002@yahoo.com.mx

 Published by Wiley-Blackwell. © 2013 The Protein Society

Keywords: Alzheimer's disease; amyloid beta peptide (Aβ); oligomerization; copper; molecular dynamics simulations

Introduction

The accumulation of insoluble amyloid "plaques" and oligomers of beta amyloid peptide (Aβ) in the brain plays an important role in Alzheimer's disease (AD), which is one of the principal causes of dementia worldwide,[1] causing oxidative stress and inflammation in specific areas of the brain.[2] Amyloid fibrils and oligomers are formed by a process called amyloidosis, in which the beta-amyloid peptide (Aβ) produces insoluble aggregates. Aβ is produced from the proteolytic cleavage of amyloid precursor protein (APP) by β and γ secretases or by α and γ-secretases to initiate amyloidogenic or nonamyloidogenic pathways, respectively.[3] The length of the Aβ peptide released by β-secretase varies from 39 to 43 amino acid residues, with the 42 amino acid residue peptide ($A\beta_{1-42}$) being the most commonly found in fibrils. $A\beta_{1-42}$ is composed primarily of hydrophobic amino acid residues at the C-terminal end,[4] which establish hydrophobic interactions during the oligomerization and fibrillization process. Furthermore, during these processes, the β-sheet conformation is defined and stabilized by the formation of an intrachain and interchain salt bridge between Asp 23/Glu 22 and Lys 28, increasing the ability of Aβ to nucleate and form fibrils.[5]

Because of the toxicity of $A\beta_{1-42}$ oligomers and fibrils, the prevention of amyloidosis could have an enormous impact on the treatment of AD. Several studies have explored the use of metals and small compounds as oligomerization inhibitors, but a molecular-level understanding of the inhibition mechanism remains unclear. One of the metals that has attracted attention is copper (Cu^{2+}), whose concentration is threefold greater in AD patients than in normal patients, with concentrations between 340 and 400 μ*M*.[6,7] The interaction between Aβ-fibrils and Cu^{2+} is important not only because of its role in amyloidosis but also because it has been associated with the generation of oxidative stress.[8] Therefore, several experimental and computational methods have focused on the analysis of the interaction between $A\beta_{1-42}$ and Cu^{2+}. However, although some research has shown that Aβ contains amino acid residues that can interact with Cu^{2+},[9] the effects of these interactions with respect to the $A\beta_{1-42}$ oligomerization process have been contradictory. Some reports have demonstrated that the presence of Cu^{2+} favors fibril formation,[10] while other recent studies suggested that Cu^{2+} might inhibit $A\beta_{1-42}$ fibril formation.[7] In addition, numerous compounds have been found to reduce $A\beta_{1-42}$ aggregation *in vitro*.[11,12] However, the usefulness of these compounds as inhibitors of $A\beta_{1-42}$ aggregation remains speculative due to their lack of specificity and/or unknown mechanism of action. For example, galanthamine (Reminil®; AChE inhibitor) has been recently demonstrated to interact with soluble Aβ to inhibit the formation of the toxic oligomeric species in a concentration-dependent manner, but its mechanism of interaction has not been well established.[13]

Therefore, the elucidation of the mechanisms of Cu^{2+} and galanthamine inhibition of $A\beta_{1-42}$ oligomerization may be useful in the rational design of drugs for AD patients. This study therefore aimed to analyze the Cu^{2+} and galanthamine interactions with $A\beta_{1-42}$ using theoretical and experimental studies. For this purpose, we performed *in silico* studies; first, an $A\beta_{1-42}$ monomer in the α-helix conformation with and without Cu^{2+} or galanthamine was submitted to molecular dynamics (MD) simulations to evaluate the conformational change. Subsequently, docking studies were performed using the conformer of $A\beta_{1-42}$ obtained at 20 ns from the MD simulations to evaluate the interactions between the $A\beta_{1-42}$ monomers and compare them with those of $A\beta_{17-42}$, which forms the Aβ oligomers. The inhibition of the $A\beta_{1-42}$ fibril formation by Cu^{2+} and galanthamine was assessed *in vitro* using ThT fluorescence, whereas the predominant secondary conformation was investigated using circular dichroism (CD) measurements.

Results

$A\beta_{1-42}$ sequence selection

Eleven Aβ sequences were identified from the Protein Data Bank (PDB) [Fig. 1(A)]. These sequences were submitted to multiple alignment. We observed that the sequences did not contain mutations; however, some sequences were incomplete, having only the residues 1–16 (PDB code: 2BP4) or lacking of these residues (PDB codes: 1QYT, 1QXC, and 1QWP), which belong to the disordered region (DR), because the $A\beta_{1-42}$ structure has been divided into two major regions [Fig. 1(B)]. The first region comprises residues 1–17 and is characterized by its high degree of flexibility. The second region comprises residues 18–42 and is commonly known as the β-folded region (βR); it contains two intermolecular, parallel, in-register β-sheets formed from residues 18–26 (β1) and 31–42 (β2), which are connected by a turn formed by residues 27–30[14,15] [Fig. 1(B)]. As depicted in Figure 1(A), several sequences, such as 1QYT, 1QXC, and 1QWP, contained amino acids involved in the turn and the β2 region. However,

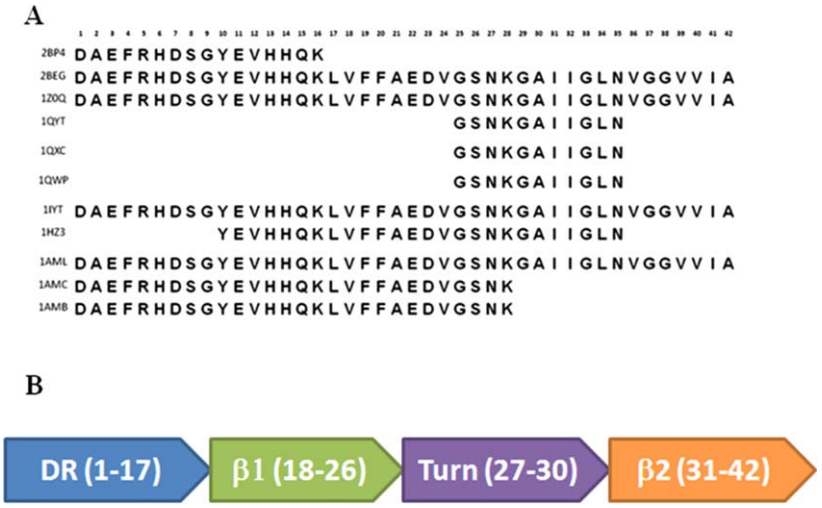

Figure 1. The $A\beta_{1-42}$ amino acid sequence and structure. (A) The alignment of Aβ sequences obtained from the Protein Data Bank. (B) A schematic representation of $A\beta_{1-42}$. Residues 1–17 comprise the disordered region (DR), residues 18–26 comprise the β1 region, residues 27–30 comprise the turn region, and residues 31–42 comprise the β2 region. [Color figure can be viewed in the online issue, which is available at wileyonlinelibrary.com.]

other structures, such as 1Z0Q, 2BEG, IIY3, and 1AML, possessed complete sequences (Abeta1-42). We chose to study 1Z0Q and 2BEG because these structures have been most frequently quoted in the literature.

Molecular dynamics simulations

MD simulation of $A\beta_{1-42}$ in the α-helix conformation. The $A\beta_{1-42}$ structure selected for the MD simulation was that with PDB code 1Z0Q, which has an α-helix conformation [Fig. 2(A)]. It gradually acquired a characteristic U-shape after 5 ns [Fig. 2(B)], forming and stabilizing the spin portion (amino acid residues 27–30), as depicted in Figure 2(C,D). The average values of the root-mean-square deviation (RMSD), the radius of gyration (Rg) and the root-mean-square fluctuations (RMSF) of the $A\beta_{1-42}$ simulation were calculated, taking into account the entire MD simulation. As displayed in Figure 2(E), the maximum RMSD value for all of the C_α atoms was ≅9 Å, and peptide convergence was reached after 6 ns, which allowed a stationary state in which the RMSD approached its maximum. The Rg values, which are a measure of the compactness of the protein, were highest during the first 6 ns and achieved convergence [Fig. 2(F)]; these results are in agreement with the views in Figure 2(B–D), where $A\beta_{1-42}$ acquires the characteristic U-shaped architecture and the β-turn after 5 ns. These structural changes related to the secondary structure can be analyzed using the RMSF, which exhibit peaks that correspond to the average atomic mobility of the backbone. Based on the RMSF results, a high degree of variability was observed in the residues that comprise the turn and the β2 region, which implies that a conformational change occurred in the $A\beta_{1-42}$ structure, as shown in Figure 2(G). The formation of a salt bridge between Asp 23 and Lys 28 enabled the conformational change of $A\beta_{1-42}$, producing the β-turn. As displayed in Figure 2, the distance between these amino acids diminished considerably, from 22.02 Å at 0 ns [Fig. 2(A)] to 17.49 Å at 5 ns [Fig. 2(B)], 13.44 Å at 15 ns [Fig. 2(C)], and 5.6 Å at 20 ns [Fig. 2(D)]. The salt bridge formation allowed the amino acids at the turn to gradually acquire a β-sheet conformation. As observed in Figure 3(A), these amino acids were in an α-helix conformation at the beginning of the simulation, and Gly 29 and Lys 28 achieve a β-sheet conformation after 20 ns of simulation [Fig. 3(B)].

MD simulation of $A\beta_{1-42}$ in an α-helix with Cu^{2+}. Figure 4 illustrates the top view of the results from the MD simulation for $A\beta_{1-42}$ in the presence of Cu^{2+}. It is possible to observe that the $A\beta_{1-42}$ remained in the α-helix conformation for the entire duration of the MD simulation [Fig. 4(A–D)] and that the U shape was not observed. Furthermore, because the Cu^{2+} and His residues did not interact, the results from this MD simulation contradict those reported in the literature.[9,16,17] Consequently, we evaluated the amino acid residues that interacted with Cu^{2+}, Asp 23, and Glu 22, as displayed in Figure 4(B–D). The distance between Cu^{2+} and Asp 23 was lower (2.01 Å) compared with that between Cu^{2+} and Glu22 (4.81 Å) at the end of the simulation [Fig. 4(D)].

The coordination geometry of Cu^{2+} is typically tetrahedral, where Cu^{2+} can interact with up to four water molecules; however, it has also been reported that Cu^{2+} can interact with amino acid residues other than His.[16,17] Thus, for $A\beta_{1-42}$ in the α-helix conformation, Asp 23 did not interact with Lys 28,

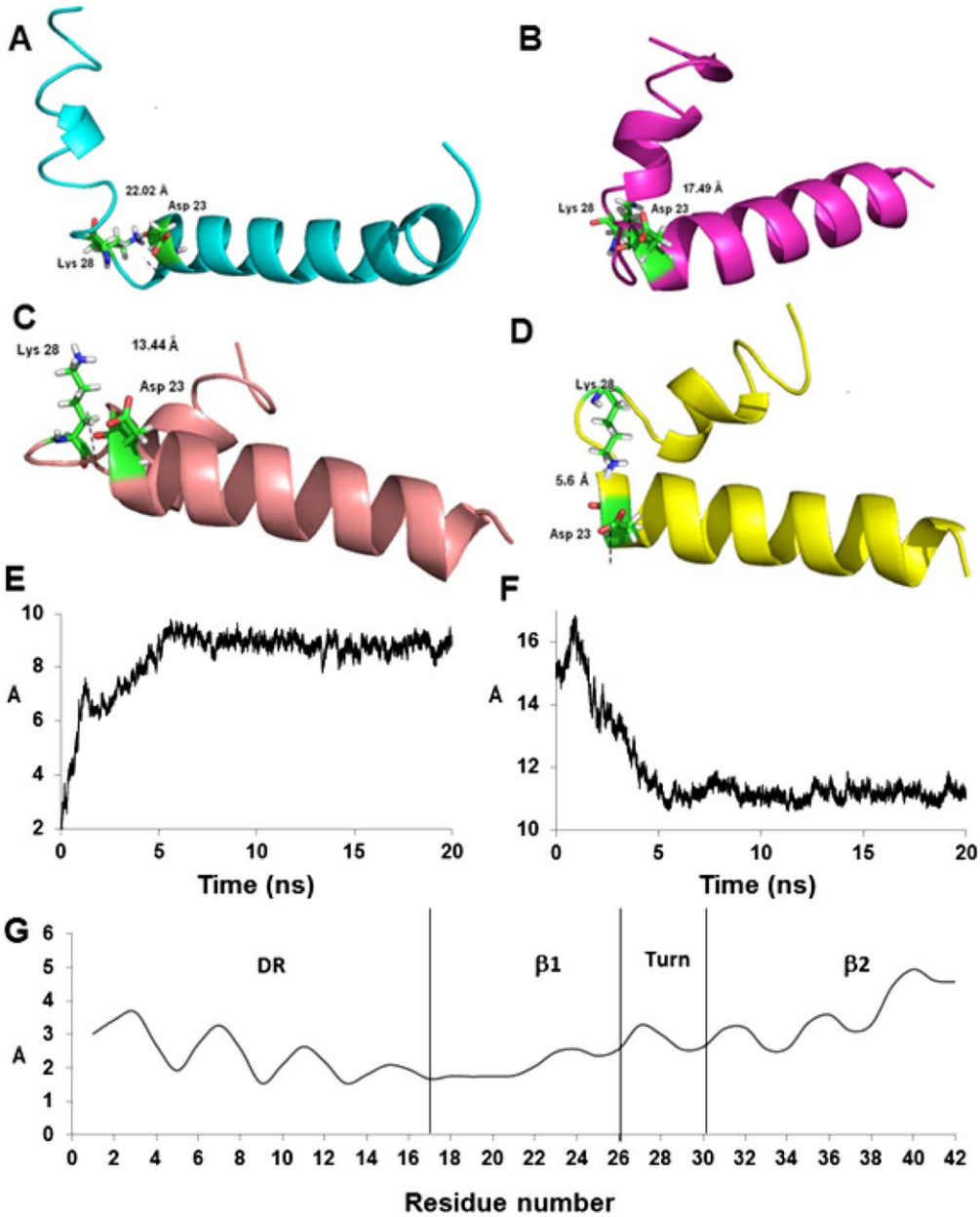

Figure 2. Results obtained from the $A\beta_{1-42}$ MD simulation. The top views of the conformers obtained at different MD simulations times: (A) 0 ns, (B) 5 ns, (C) 15 ns, (D) 20 ns, (E) RMSD, (F) Rg, and (G) RMSF. Notably, at 5 ns, $A\beta_{1-42}$ acquires a characteristic β-turn that remains constant throughout the simulation, and near this time point the RMSD reaches convergence. [Color figure can be viewed in the online issue, which is available at wileyonlinelibrary.com.]

which allowed the negatively charged zone (Asp23 and Glu22) to interact with Cu^{2+}. Furthermore, the carboxylate group can act as a bidentate ligand in coordination with copper, in which the tetrahedral geometry is conserved.

The RMSD, Rg, and RMSF values of the $A\beta_{1-42}$–Cu^{2+} interaction during the MD simulations were calculated considering the entire dynamic simulation. Figure 4(E) displays the RMSD values for all of the Cα atoms. The maximum RMSD was 5 Å; however, a variation of 2 Å was observed, indicating that conformational changes in the model occurred during the MD simulation. After 10 ns, the RMSD value approached the maximum and reached convergence, as shown in Figure 4(E). The Rg values were without slight variations throughout the simulation [in Fig. 4(F)]. Based on the RMSF results, a high degree of variability was observed for the entire $A\beta_{1-42}$ structure, as shown in Figure 4(G). The Asn 27, Asp 23, and N-terminal residues exhibited the highest mobility. No great conformational changes were observed in this MD simulation [Fig. 4(A–D)], and the turn was not formed. This result corresponds with Figure 3(C), where after 20 ns of simulation in the presence of Cu^{2+}, the amino acids at the turn location remain in an α-helix conformation.

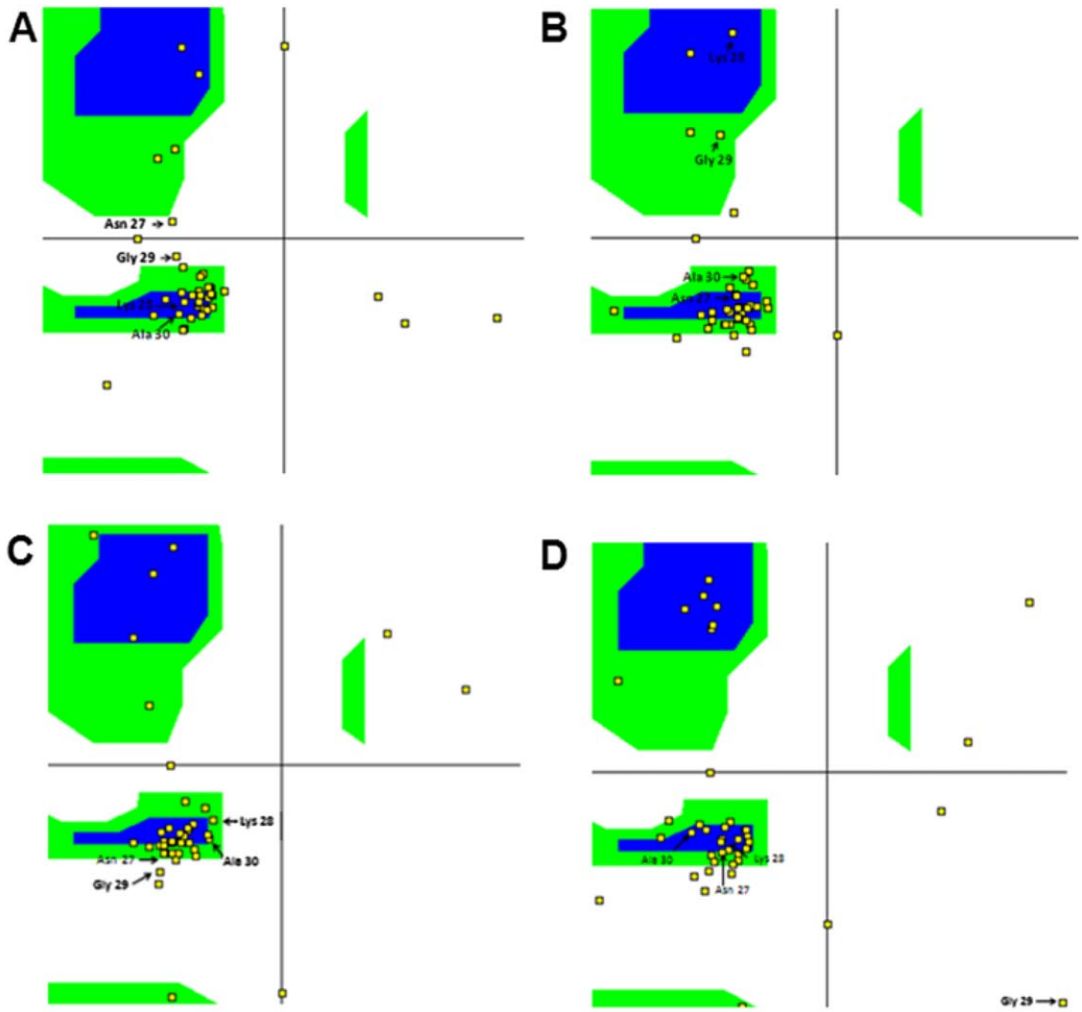

Figure 3. Ramachandran plots of $A\beta_{1-42}$ conformers obtained from the MD simulations. $A\beta_{1-42}$ in an α-helix conformation at time 0 ns (A) and 20 ns (B); $A\beta_{1-42}$ in the presence of Cu^{2+} (C) and galanthamine (D) after 20 ns of simulation. The amino acids that comprise the turn have been identified. As shown in the figure, the amino acids gradually adopt a β-sheet conformation, but in the presence of Cu^{2+} or galanthamine, the conformational change does not occur. [Color figure can be viewed in the online issue, which is available at wileyonlinelibrary.com.]

MD simulation of $A\beta_{1-42}$ in a β-folded conformation with Cu^{2+}. To evaluate the effect exerted by Cu^{2+} on $A\beta_{1-42}$ in the β-folded conformation, a 20-ns MD simulation was performed. The coordinates for $A\beta_{1-42}$ were taken from the results of the $A\beta_{1-42}$ simulation without Cu^{2+} at 13 ns (structure refinement). Although the Cu^{2+} was located near the reported specific amino acid interaction (His 6, 13, and 14), it exhibited a tendency to move toward the negatively charged side chains of Glu 22 and Asp 23 [Fig. 5(A–D)]. The interaction between Cu^{2+} and Glu22 and Asp23 prevented the secondary conformational change as well as the gradual loss of the U shape [Fig. 5(D)].

Figure 5(E) demonstrates that the maximum RMSD value for all of the Cα atoms was 8 Å, with the occurrence of wide variations that demonstrate that the conformational changes were induced by Cu^{2+}. In contrast, the Rg value was not stable at any point during the simulation [Fig. 5(F)]. The RMSF results indicate a high degree of variability, especially for the DR [Fig. 5(G)].

MD simulation of $A\beta_{1-42}$ with galanthamine. The top view in Figure 6 displays the results from the MD simulation of $A\beta_{1-42}$ with galanthamine. $A\beta_{1-42}$ was in the α-helix conformation at the beginning of the simulation [Fig. 6(A)] and gradually acquired a U-shaped structure [Fig. 6(B,C)]. As shown in Figure 6(D), the principal interaction between galanthamine and $A\beta_{1-42}$ involved the π-cation with Lys 28 whereas the N atom positively charge of galanthamine make a salt bridge with Asp 23.

The RMSD, Rg, and RMSF values of the interaction between $A\beta_{1-42}$ and galanthamine were calculated for the entire MD simulation. As displayed in Figure 6(E), the maximum RMSD value for all of the C_α atoms was 9 Å. The protein reached

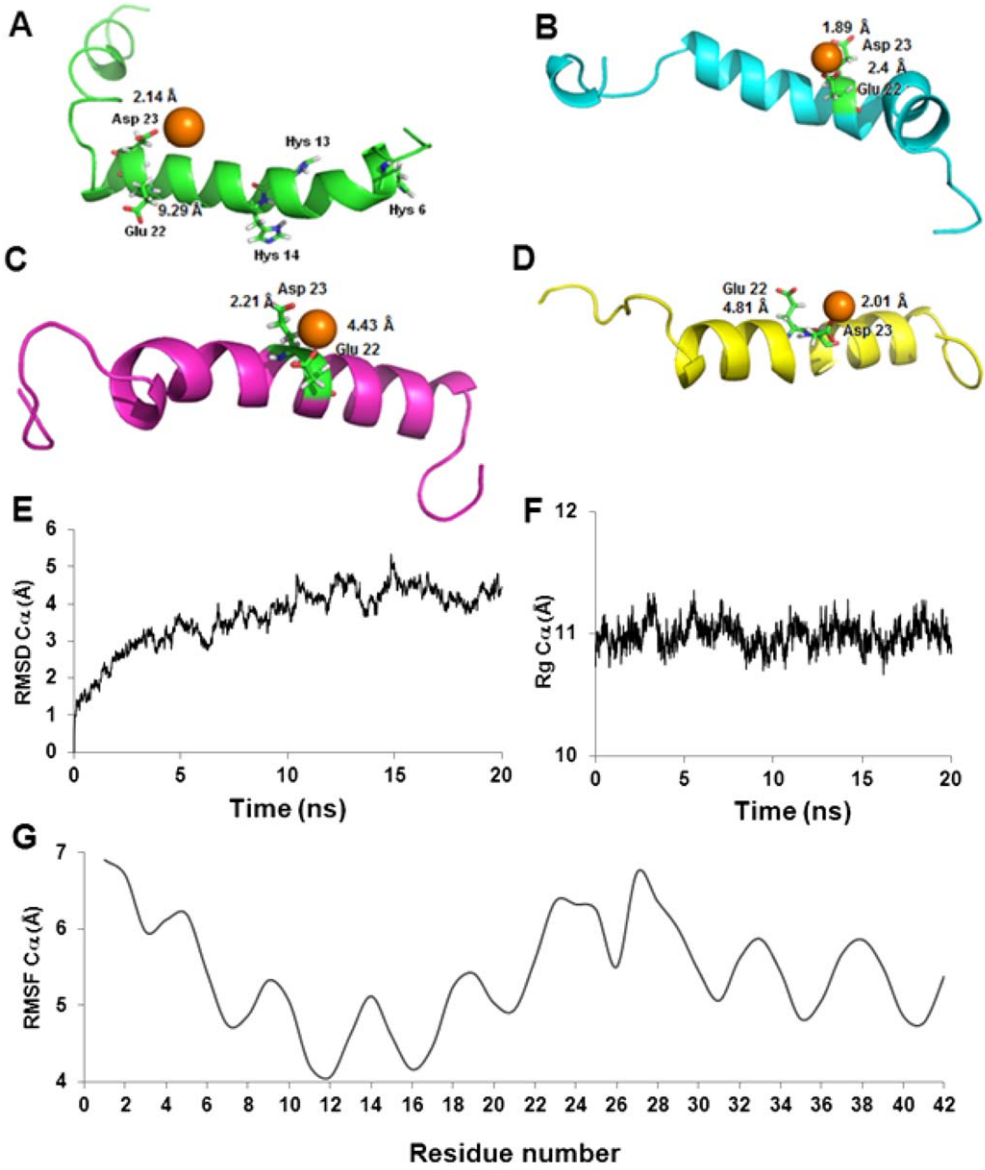

Figure 4. Results obtained from the $A\beta_{1-42}$ α-helix MD simulation in the presence of Cu^{2+}. The top views of the conformers at various simulation times are shown. (A) Time 0, (B) 5 ns, (C) 15 ns, (D) 20 ns, (E) RMSD, (F) Rg, (G) RMSF. As evident from the results, no conformational changes were observed, in contrast to $A\beta_{1-42}$ without Cu^{2+}. [Color figure can be viewed in the online issue, which is available at wileyonlinelibrary.com.]

convergence at ≅6 ns, where the RMSD approached its maximum, which was then maintained throughout the remainder of the MD simulation. The Rg was stable at 12 Å in the complete simulation [Fig. 6(F)]. Based on the RMSF results, the residues that comprised the DR exhibited a large variability [Fig. 6(G)]. The Ramachandran plot at 20 ns revealed that the amino acids located at the turn remained in an α-helix conformation [Fig. 3(D)].

Docking studies. For docking studies, we used the 2BEG structure (residues 17–42) and a snapshot conformer of $A\beta_{1-42}$ obtained by MD simulations at 20 ns (PDB code: 1Z0Q, a complete 3D structure). Both structures have the minimal sequence able to form the oligomers.[18] Therefore, the protein–protein docking was first performed with two monomers of each structure to build a dimer (Fig. 7, Set 1, in blue). From these studies, according to the Clus Pro 2.0 server, four main interactions were observed between the monomers, which were induced by (a) all types of interactions, known as balanced; (b) hydrophobic forces; (c) electrostatic forces; and (d) Van der Waals interactions (VdW).[19,20]

An analysis of the interactions between the oligomers obtained using the conformer from the MD simulation of the 1Z0Q and 2BGE structures revealed different orientations, including dimers (Fig. 7, Set 1 in color blue), trimers (Fig. 7, Set 2 in color green), tetramers (Fig. 7, Set 3 in color pink),

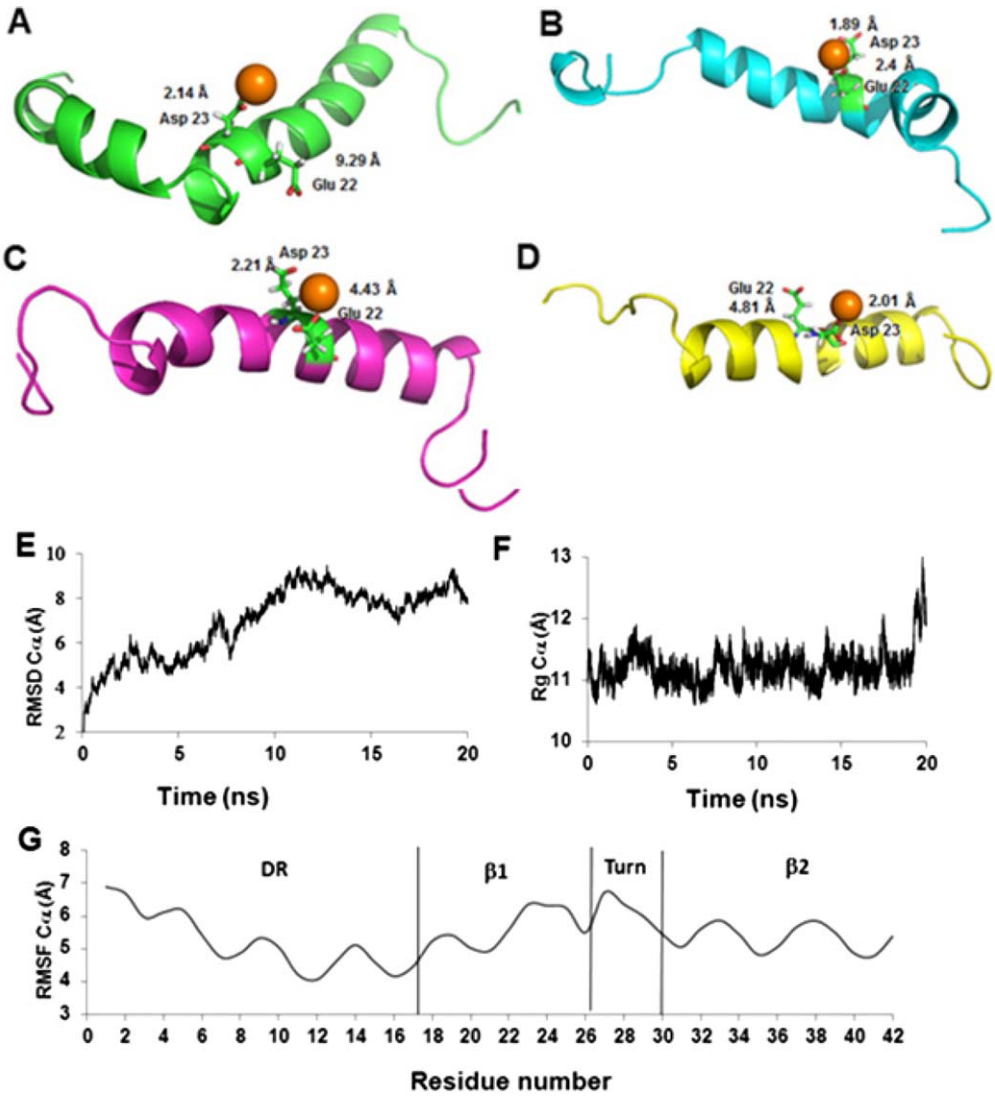

Figure 5. Results obtained from the MD simulation of $A\beta_{1-42}$ in the β-sheet conformation with Cu^{2+}. The top views of the conformers at various times are shown. (A) Time 0, (B) 5 ns, (C) 15 ns, (D) 20 ns, (E) RMSD, (F) Rg, (G) RMSF. As evident from the figure, the presence of Cu^{2+} induces the loss of the β-sheet conformer of $A\beta_{1-42}$ and the formation of the α-helix conformer. [Color figure can be viewed in the online issue, which is available at wileyonlinelibrary.com.]

and pentamers (Fig. 7, Set 4 in color orange), that depended on the type of interaction present. However, only the oligomers formed by hydrophobic interactions exhibited unidirectional growth along the axis.

These oligomers were subsequently used to analyze interchain interactions, such as hydrogen bonds, that formed between the backbone of residues Val 39–Val 18, Asp 23–Leu 34, Lys 28–Val 36, Glu 22–Met 35, and Phe 20–Gly 37 and that were constant in all of the oligomers (Table I). Importantly, other interactions were observed in the oligomer (Gly 38–Phe19, Gly 38–Val 39, Ile 32–Gly25, Leu 17–Val 40 for the trimer, and Val 36–Ala 21 for the tetramer). Furthermore, salt bridge (Asp23–Lys28) formation was observed in both structures (2BEG and 1Z0Q conformer 20 ns from MD), and the formation of these salt bridges induced interactions between neighboring hydrophobic side chains [Fig. 7(E)]. As outlined in Table I (1Z0Q conformer), this salt bridge was present in all of the oligomers and was shorter in length when more Aβ chains were present. However, in the structure 1Z0Q, additional interactions between the monomers, such as electrostatic interactions between Asp 7 and Lys 16, were observed due to the presence of the DR [Fig. 7(F)]. In addition, in the 1Z0Q structure, the interchain hydrogen bonds between the backbone of the amino acid residues Met35–Val40, Arg5–Tyr10, Glu11–Hys6, Val36–Ile41, Ile31–Val36, and Phe20–Gln15 remained constant in all of the oligomers; importantly, other hydrogen bonds were added and remained constant in the subsequent higher order oligomer (Ala30–Met35 in the trimer and Phe19–His14 and Phe19–His14 in the tetramer).

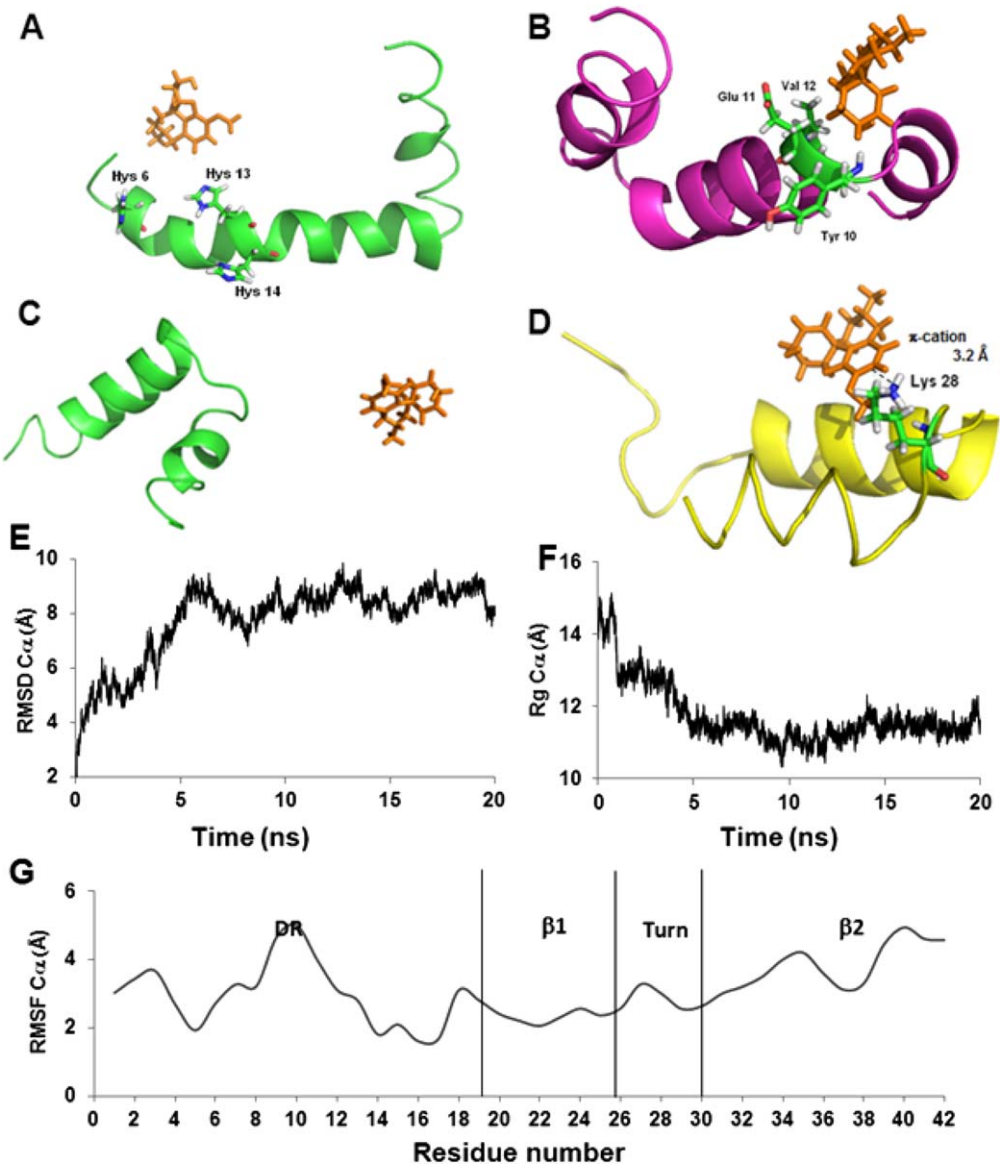

Figure 6. Results obtained from the $A\beta_{1-42}$-galanthamineMD simulation. The top views of the conformers at various MD simulation times: (A) time 0, (B) 5 ns, (C) 15 ns, (D) 20 ns, (E) RMSD, (F) Rg, (G) RMSF. Galanthamine did not interact with $A\beta_{1-42}$ during the simulation. Significantly, at 20 ns, galanthamine was observed to form a π-cation interaction with Lys 28. [Color figure can be viewed in the online issue, which is available at wileyonlinelibrary.com.]

Evaluation of $A\beta_{1-42}$ aggregation by thioflavin T fluorescence

Monitoring the in vitro formation of $A\beta_{1-42}$ fibrils. The fluorescence signal of thioflavin T (ThT) has been well documented to increase when ThT is bound to amyloid structures; therefore, this signal can be used to evaluate the formation of misfolded protein aggregates.[21] For this experiment, nonfibrillated $A\beta_{1-42}$ peptide was used as the starting material to monitor the fibrillization process. The experimental conditions for $A\beta_{1-42}$ fibrillization have been described in previous reports.[7] The increase in the intensity of the fluorescence signal of ThT associated with $A\beta_{1-42}$ fibrillization is depicted in Figure 8(A). The time course for the formation of the fibrils was also observed through continuous monitoring of the changes in the ThT fluorescence intensity at 480 nm over the course of 24 h; this time period is sufficient to allow fibril formation under incubation and stirring conditions. A rapid increase in the ThT fluorescence signal is demonstrated in Figure 8(B), which depicts a two-phase-growth curve that is typical of amyloid fibril formation. When $A\beta_{1-42}$ was incubated without agitation, the fibrillization process was extremely slow, and the increase was only observed after prolonged incubation (data not shown).[22]

Effects of Cu^{2+} and galanthamine on the formation of $A\beta_{1-42}$ fibrils. Both Cu^{2+} and galanthamine inhibited $A\beta_{1-42}$ fibrillization, as depicted in

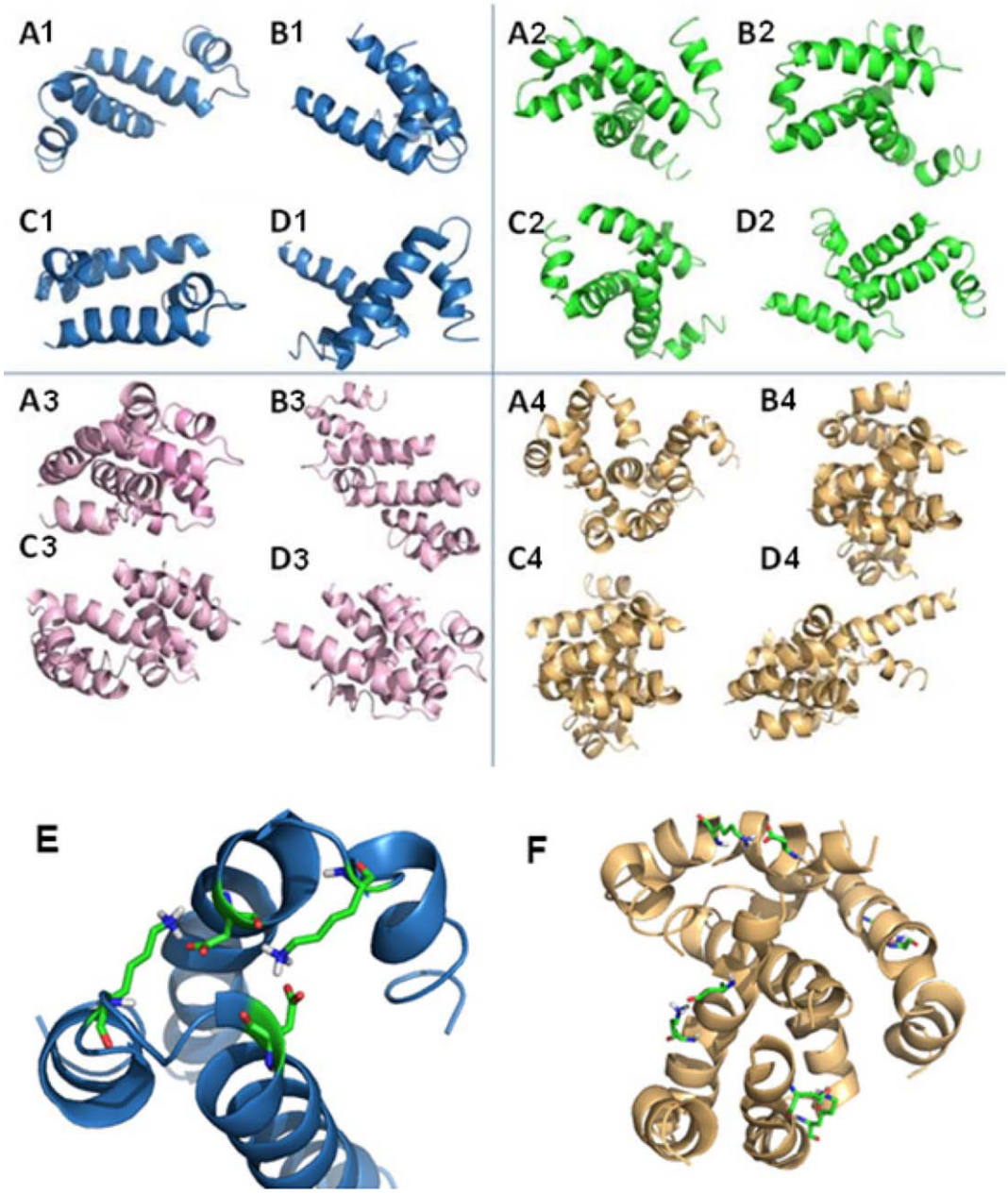

Figure 7. $A\beta_{1-42}$ oligomers obtained by docking using using a snapshot of Abeta1-42 obtained by MD simulations at 20 ns (PDB code: 1Z0Q). In each set of figures, the letter represents a type of interaction: (A) all types of interactions, known as balanced; (B) hydrophobic interactions; (C) electrostatic forces; (D) van der Waals forces. For the dimer (Set 1, in blue), trimer (Set 2, in green), tetramer (Set 3, in pink), and pentamer (Set 3, in orange). (E) A schematic representation of the formation of the salt bridge between Asp 23 and Lys 28 in the dimer. (F) A schematic representation of the formation of another salt bridge between Asp 7 and Lys 16 in the pentamer. [Color figure can be viewed in the online issue, which is available at wileyonlinelibrary.com.]

Figure 8 (panels A and B). The addition of Cu^{2+} prevented $A\beta_{1-42}$ fibrillization, as demonstrated by the small increase in the ThT fluorescence signal following Cu^{2+} addition. The addition of galanthamine also decreased the fibrillization process, but the effect was not as pronounced as that observed for Cu^{2+}. These observations are in good agreement with the MD simulation results, in which Cu^{2+} exhibited a high affinity for the Glu 22 and Asp 23 side chains, as demonstrated by the proximity of Cu^{2+} to these amino acid residues throughout the duration of the simulation. In comparison, galanthamine interacted weakly with Lys 28 in $A\beta_{1-42}$; however, this interaction was sufficient to prevent the fibril formation process, as demonstrated by the fluorescence results.

Circular Dichroism

Figure 9 displays representative CD spectra of $A\beta_{1-42}$ alone and in the presence of Cu^{2+} or galanthamine following 1 h of incubation; the spectra were corrected for ellipticity using the CD spectra of Cu^{2+}

Table I. *Interactions Encountered in the Aβ$_{1–42}$ (PDB code 1Z0Q) Oligomers Obtained by Docking Studies*

Dimer	Trimer	Tetramer	Pentamer
Salt Bridge	Salt Bridge	Salt Bridge	Salt Bridge
Asp 23-Lys 28 1.88[a]	Asp 1-Lys 28 2.77[a]	Asp 23-Lys 28 2.98[a]	Asp 23-Lys 28 1.79[a]
Asp 23-Lys 28 2.44[a]		Asp 23-Lys 28 2.43[a]	Asp 23-Lys 28 1.28[a]
Lys 16-Asp 7 1.77[a]	HYDROGEN BONDS	Asp 23-Lys 28 3.28[a]	Asp 23-Lys 28 2.84[a]
	Ile41 H-Val36 O (1.81)	Asp 23-Lys 28 2.98[a]	Asp 7-Lys 16 1.7[a]
HYDROGEN BONDS	Ile 31 O-Val36 H (1.81)	Asp7-Lys16 1.82[a]	Asp 7-Lys 28 3.13[a]
Met 35 O- Val 40 H (1.86)	Val40 H-Met35 O (1.89)	Lys16-Asp7 2.54[a]	Asp 7-Lys 16 1.7[a]
Glu 11 O- Tyr 10 (1.99)	Arg5 H-Asp10 O (2.0)		Asp 7-Lys 16 1.28[a]
Asn27 H–Val 24 O (2.02)	Asp7 H-Glu3 O (1.95)	HYDROGEN BONDS	Asp 7-Lys 16 2.84[a]
Ser26 H-Glu22 O (1.94)	Lys28 H-Val24 O (1.97)	Ile41 H-Val38 O (1.81)	
Gln15 O-Tyr10 H (1.92)	Val18 O-Asp23 H (1.88)	Val36 H-Ile31 O (1.81)	HYDROGEN BONDS
Tyr10 O-Arg5 H (1.87)	Met35 H-Ala 30 O (1.87)	Val40 H-Met35 O (1.89)	Val24 O-Asn27 H (2.01)
Asp7 H-Glu3 O (1.73)	Val 40 H-Met35 O (1.91)	Arg5 0-Tyr10 H (1.86)	Ser26 H-Glu22 O (1.95)
Glu11 H-His6 O (1.95)	Lys16 O-Ala21 H (1.86)	Glu22 O-Asp7 H (1.73)	Phe19 O-Val24 H (1.86)
Tyr10 H-Glu11 O (1.91)	Phe20 H-Gln15 O (1.91)	Asp1 H-Glu3 O (1.95)	Asp1 O-Arg5 H (1.92)
Lys16 H-Glu11 O (1.9)	Val24 H-Phe19 O (1.86)	Hys6 O-Glu11 H (1.96)	Ile31 O-Val36 H (1.82)
Val36 O-Ile41 H (1.82)	His6 O-Glu11 H (1.85)	Glu11 O-Lys16 H (1.96)	Val36 O-Ile41 1.81 (1.81)
Met35 O-Val40 H (1.89)	His6 H-Tyr10 O (2.03)	Tyr10 O-Gln15 H (1.92)	Phe19 H-His14 O (1.84)
Ile31 O-Val36 H (1.81)	Ser8 O-His13 H (1.93)	Lys16 O-Ala21 H (1.86)	Gln15 H-Tyr10 O (1.92)
Ala21 H-Lys16 O (1.86)	Val40 H-Met35 O (1.83)	Gln15 O-Phe20 H (1.94)	Met35 O-Val40 H (1.89)
Phe20 H-Gln15 O (1.91)	Glu11 O-Lys6 H (1.89)	Tyr10 H-Glu11 O (2.03)	Tyr10 H-Arg5 O (1.88)
Val24 H-Phe19 O (1.86)	His6 H-Glu11 O (1.95)	Phe19 H-Hys14 O (2.85)	Met35 O-Val40 H (1.86)
	Glu3 O-Asp7 H (1.73)	Val24 H-Phe19 O (1.86)	Phe20 H-Gln15 O (1.91)
	Arg5 H-Asp1 O (1.88)	Ser26 H-Glu22 O (1.96)	Glu11 O-Tyr10 H (2.03)
	His14 H-Gly9 O (1.87)	Asn27 H-Val24 O (2.01)	Ala21 H-Lys16 O (1.96)
	Lys28 H-Val24 O (1.94)	Val40 H-Met35 O (1.86)	Val18 H-His3 O (1.88)
	Phe20 H-Gln15 O (1.85)	Ile41 H-Val36 O (1.85)	Phe19 H-His14 O (1.97)
	Glu22 O-His6 H (1.98)	Phe4 O-Gly9 H (1.96)	Lys16 H-Glu17 O (1.89)
		Asp7 O-Arg5 H (1.75)	Arg5 H-Glu11 O (1.93)
		Gly37 H-Ile32 O (1.93)	Glu11 H-His6 O (1.95)
		His13 O-Val18 H (1.97)	Glu3 O-Asp1 H (2.01)
		Glu22 O-Lys28 H (1.75)	His6 H-Ala2 O (1.85)
		Lys28 H-Glu22 O (1.81)	Gly29 H-Ser26 O (2.01)
		Glu22 O-Ser26 H (1.9)	Ser26 H-Glu22 O (1.87)
		Asp23 O-Lys28 H (1.65)	Val40 H-Met35 O (1.92)
		Val24 O-Asn27 H (1.96)	Met35 O-Val40 (1.9)
		Hys6 O-Glu11 H (1.93)	Lys28 H-Asp7 O (1.81)
		Tyr10 O-Gln15 H (1.85)	Glu3 O-Asp7 H (1.74)
		Met35 H-Ala30 O (1.95)	His14 H-Gly9 O (1.92)
		Val18 O-Glu22 H (1.96)	His6 H-Ala2 O (1.96)
		Lys16 H-Tyr10 O (1.63)	Glu11 O-Tyr10 H (1.93)
		Lys16 H-Glu11 O (1.71)	Tyr10 H-Glu11 O (1.91)
		Val40 H-Met35 O (1.86)	Val12 H-Asp7 O (1.91)
		Leu34 H-Gly29 O (1.93)	Val18 H-His13 O (1.9)
		Tyr10 H-Glu11 O (1.9)	Gln15 O-His14 H (1.9)
		Val18 O-Asp23 H (1.94)	Phe19 H-His4 O (1.95)
		His14 O-Phe19 H (1.94)	Lys16 H-Glu11 O (1.88)
		Leu17 O-Glu22 H (1.92)	Asn27 H-Val24 O (1.93)
		His13 O-Val18 H (1.98)	Leu17 O-Ala21 H (1.92)
		Gly9 O-His14 H (1.97)	Asp23 O-Asp14 H (1.94)
		Ser8 O-His13H (1.91)	Ala30 O-Met35 H (1.94)
		Phe4 O-Gly9 H (1.94)	Phe19 H-His14 O (1.82)
		His6 O-Glu11 H (1.93)	Ser26 H-Glu22 O (1.92)
		Glu11 O-Lys16 H (1.94)	Glu11 O-Lys16 H (1.72)

[a] Distances are presented in Å.

or galanthamine. After the sample was incubated for 1 h under conditions that favored fibril formation, the CD spectrum revealed changes in the secondary structure, which indicated the formation of the β_I conformation for Aβ$_{1–42}$. When Aβ$_{1–42}$ was incubated in the presence of either Cu^{2+} or galanthamine, the CD spectra in both cases indicated a very high proportion of β_{II} content (68 and 67%, respectively) and a significant reduction in the proportion of β_I (Table II).

Discussion

The formation of Aβ fibrils and oligomers is one of the major pathological hallmarks of AD.[23] These

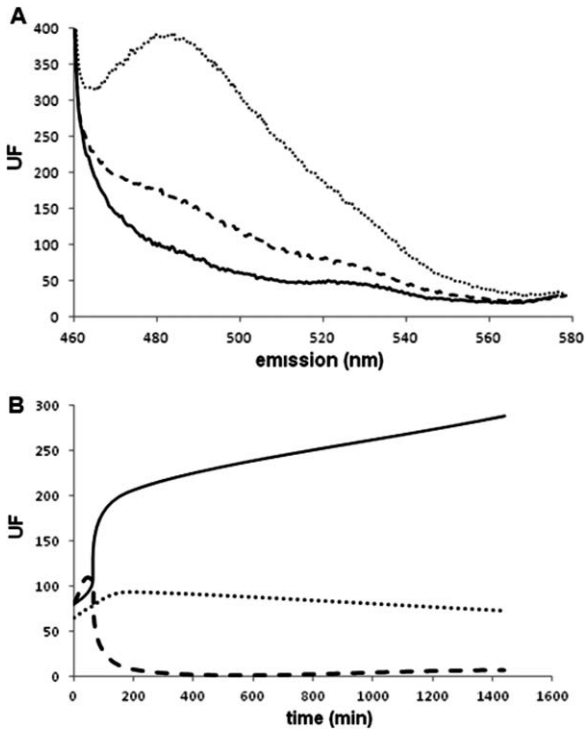

Figure 8. Effect of compounds on $A\beta_{1-42}$ fibrillization, analyzed using the fluorescence intensity of ThT in the presence of Cu^{2+} and galanthamine after 24 h of incubation: (A) 0.9 μ*M* $A\beta_{1-42}$ (dotted line), 0.9 μmol/L $A\beta_{1-42}$ in the presence of 20 μ*M* Cu^{2+} (continuous line), 0.9 μ*M* $A\beta_{1-42}$ in the presence of 100 μmol/L galanthamine (dashed line). (B) Emission at 480 nm of $A\beta_{1-42}$ (continuous line), $A\beta_{1-42}$ and Cu^{2+} (dashed line), and $A\beta_{1-42}$ and galanthamine (dotted line).

fibrils have been shown to produce reactive oxygen species (ROS) such as H_2O_2 *in vitro* as well as $^{\bullet}OH$ in the presence of transition metals such as Cu^{2+}, establishing a permanent state of oxidative stress.[8] This oxidative stress affects the cholinergic transmission system, which explains the underlying cholinergic deficit in AD patients.[24]

Several efforts have been made to elucidate the mechanism of ROS production due to the interaction of Aβ fibrils and Cu^{2+};[8] however, the effect of Cu^{2+} and other metals on the oligomerization process is not well defined, and different authors have reported contradictory results. Some reports have demonstrated that Cu^{2+} favors the aggregation of $A\beta_{1-42}$. However, in recent experiments, the incubation of $A\beta_{1-42}$ in the presence of Cu^{2+} resulted in decreased Aβ fibril formation, although no explanation for these processes at the atomistic level has been provided.[11–13]

Although several theoretical and experimental studies have been conducted with the aim of explaining the interaction of Cu^{2+} and Aβ, several contradictory results have emerged.[16] These contradictions might be explained by the different experimental conditions used by different research groups, which have included different pH values,[23] different

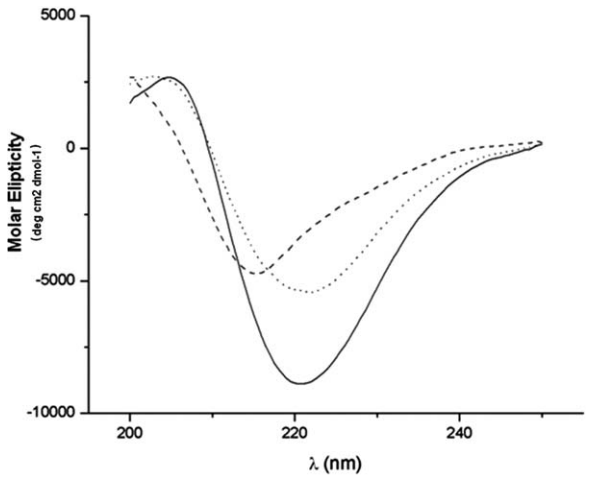

Figure 9. CD spectra of $A\beta_{1-42}$ after 1 h of incubation alone (50 μ*M*; continuous line) and in the presence of Cu^{2+} (20 μ*M*; dotted line) or galanthamine (100 μ*M*; dashed line).

types of peptides, and differences in the form in which Cu^{2+} could be coordinated to Aβ;[17] all these conditions can influence Aβ aggregation.

MD simulations were performed for the 1Z0Q structure and Cu^{2+} to elucidate the process by which Cu^{2+} prevents $A\beta_{1-42}$ fibril formation. From the results of this study, we demonstrated that, in the absence of Cu^{2+}, Aβ suffered conformational changes. At 5 ns of the MD simulation, the Aβ adopted a U-turn shape that encouraged the interaction between Asp 23 and Lys 28, as reported previously.[25] This adoption of a U-turn shape also indicated the beginning of the transformation to a β-sheet structure, which is a crucial step in initiating the oligomerization process.

However, in the MD simulation of $A\beta_{1-42}$ with Cu^{2+}, we did not observe a significant change in conformation, and the Asp 23 and Lys 28 residues remained distant throughout the simulation. In fact, for nearly the entire simulation, Cu^{2+} interacted with Glu 22 and Asp 23. This behavior was likely observed because Cu^{2+} is a cation metal and is attracted to negatively charged molecules, such as the carboxylate groups present in the side chains of the amino acid residues in $A\beta_{1-42}$. Importantly, some authors have reported that Cu^{2+} is associated with $A\beta_{1-42}$ in the β-folded structure and is tetracoordinate with three amino acid residues, including His 6, His 13, and His 14, and a fourth component

Table II. *The Proportions of the $A\beta_{42}$ Secondary Structure Induced by 20 μM Cu^{2+} and 100 μM Galanthamine, Sampled After 1 h of Incubation*

	α (%)	β_I (%)	β_{II} (%)	Error (%)
Aβ	7	87	6	3
Aβ−Cu^{2+}	20	12	68	5
Aβ−Gal	18	15	67	2

represented by a residual oxygen donor—possibly Asp or Tyr. However, these studies began with $A\beta_{1-42}$ in a β-helix conformation, and the salt bridge between Asp 23 and Lys 28 was formed. In addition, these authors observed that the change in the β-sheet folding occurred within picoseconds and that the interaction with Cu^{2+} occurred following the conformational shift.[26] Furthermore, because $A\beta_{1-42}$ is composed principally of hydrophobic amino acid residues, the amino acids that can interact with Cu^{2+} are limited to Glu 22 and Asp 23. Moreover, for $A\beta_{1-42}$ in the β-sheet conformation, the presence of the salt bridge between Asp 23 and Lys 28 prevents the interaction of these residues, favoring the interaction of Cu^{2+} with the imidazole ring of histidine. In fact, the coordination of Cu^{2+} with the imidazole rings of histidine was demonstrated in $A\beta_{1-42}$ fibrils, in which the β-sheet conformation is stabilized by the salt bridge between Asp 23 and Lys 28.[9] However, as reported in the MD simulation in this work, for $A\beta_{1-42}$ (α-helix)–Cu^{2+}, due to the absence of a salt bridge, the Cu^{2+} is free to interact with Glu 22 and Asp23. In addition, many of the studies in which Cu^{2+} was reported to interact with the histidine residues of Aβ were performed using $A\beta_{1-16}$[27] Additionally, the RMSD plots and rotation of the C_α revealed the presence of significant instability in the $A\beta_{1-42}$ chain, implying that this type of interaction promotes the destabilization of the peptide and prevents the formation of the salt bridge necessary for the transition to a β-sheet conformation. In fact, the $A\beta_{1-42}$ (β-sheet)–Cu^{2+} simulation revealed that Cu^{2+} possesses the ability to destabilize the β-sheet conformation of $A\beta_{1-42}$. This destabilization may be useful in explaining the results of the experiments in which the incubation of Aβ with Cu^{2+} inhibited Aβ aggregation.

Based on the MD simulation results for $A\beta_{1-42}$ with galanthamine, galanthamine binds to $A\beta_{1-42}$ in two different manners: the aromatic ring of galanthamine interacts with Lys 28 of $A\beta_{1-42}$ via π-cation interactions, and the protonated tertiary amine interacts with Asp 23 via electrostatic interactions, preventing the formation of the salt bridge that was shown to form before the $A\beta_{1-42}$ conformational change. Both types of interactions are capable of preventing the $A\beta_{1-42}$ conformational change from α-helix to β-sheet; according to previous reports,[28] galanthamine interacts with the amino acids located at the turn portion of $A\beta_{1-42}$, such as Lys 28. However, the affinity of $A\beta_{1-42}$ for galanthamine is lower than that for Cu^{2+}, as revealed by the higher concentration of galanthamine (100 μ*M*) necessary to inhibit the oligomerization process[13] compared with Cu^{2+} (20 μ*M*). This difference in affinity has been corroborated in this study, in which only Cu^{2+} was capable of decreasing the maximum ThT fluorescence following incubation with $A\beta_{1-42}$.

In addition, for the docking studies, the structures of $A\beta_{17-42}$ (PDB code 2BEG) and $A\beta_{1-42}$ (conformer obtained from MD at 20 ns) were used to evaluate whether the structure obtained by MD could form oligomers in the same manner as the 2BGE structure and whether amino acid residues 1–16 were important in the salt bridge formation between Asp23 and Lys28. The results from the docking study between the monomers from the 1Z0Q conformer and the 2BEG structure revealed that the addition of consecutive Aβ monomers can occur in different ways, resulting in a wide variety of associations dependent on the main type of interactions present. Thus, the large number of interactions that $A\beta_{1-42}$ can establish with other monomers with a small free energy allows the formation of different types of Aβ aggregates. Because these aggregates are strongly affected by their environment, the competing influences of the fragment interactions and the key nucleation sites may determine the polymorphic oligomer (and fibril) outcome, particularly with respect to the parallel/antiparallel backbone alignment.[29] However, not all types of aggregates are important, as demonstrated in the case of senile plaques, in which $A\beta_{1-42}$ primarily forms fibrils in the toxic form.[23] Moreover, the process by which the oligomers form hydrophobic interactions most closely resembles the oligomerization process reported for the formation of Aβ fibrils; these types of interactions might explain the low hydrophilicity of Aβ following fibril formation. Notably, although the Aβ monomers from the 2BEG structure lacked the 1–16 region, the oligomers obtained were similar in structure, conformation and behavior to the oligomers obtained from the 1Z0Q structure, which might indicate that the DR is not essential in the oligomerization process. However, for the complete Aβ sequence (1Z0Q structure), more electrostatic interactions were observed in the presence of the DR.

Additionally, experimental CD studies confirmed the computational results, revealing that Cu^{2+} and galanthamine can prevent the $A\beta_{1-42}$ conformational change and allow the predominance of amino acids in an unfolded conformation, as demonstrated by the resemblance of the spectra to the CD spectra of β_{II} proteins.[30] This conformation prevents $A\beta_{1-42}$ oligomerization, as demonstrated by the fluorescence results.

Based on these results, we concluded that three important characteristics should be considered in the rational design of $A\beta_{1-42}$ fibrillogenesis inhibitors: the presence of hydrophobic groups, aromatic rings or charged groups that can interact with Glu 22 and Asp 23 or Lys 28—characteristics that galanthamine possesses because it contains a tertiary amine capable of being protonated at physiological pH; a positive charge capable of interacting via electrostatic interactions with Asp 23; and aromatic rings capable of interacting with Lys 28 via π-cation

interactions. However, this molecule inhibits $A\beta_{1-42}$ fibril formation only weakly due to its large size. Consequently, steric hindrance effects should be considered during the design of new molecules because these effects may contribute to the ineffectiveness of these molecules as inhibitors of $A\beta_{1-42}$ fibril formation.

Conclusions

From *in silico* studies, we found that Cu^{2+} is able to prevent and revert the $A\beta_{1-42}$ secondary-structure conformational change by interacting with Glu 22 and Asp 23 to prevent the formation of a salt bridge. In comparison, galanthamine, which bound to $A\beta_{1-42}$ via π–cation interactions with Lys 28, also inhibited salt-bridge formation, but by a different mechanism. The inhibition of the $A\beta_{1-42}$ fibrillation process was observed using ThT fluorescence. In addition, this inhibition was further confirmed using CD spectroscopy.

Methods

Aβ sequence selection

To use the most complete three-dimensional (3D) Aβ structure without mutations or missing residues, a search in the Protein Data Bank (PDB) (http://www.rcsb.org/pdb/home/home.do) was performed, which identified 11 structures (PDB codes: 2BP4, 2BEG, 1Z0Q, 1QYT, 1QXC, 1QWP, 1IYT, 1HZ3, 1AML, 1AMC, 1AMB). A multiple alignment was performed using the STRAP program (http://www.bioinformatics.org/strap/), and the results were edited to find similarities and differences in the sequences.

Molecular dynamics simulations

The native $A\beta_{1-42}$ monomer was used for the MD simulations. The calculations were performed using the structure of $A\beta_{1-42}$ (PDB code: 1Z0Q model 1) determined by Tomaselli *et al.*[31]

MD simulation of $A\beta_{1-42}$ in an α-helix structure. MD simulations were performed with the NAMD 2.6 software package.[32] Hydrogen atoms were added with the psfgen command within the VMD program[33], and the structure was minimized using the steepest descent algorithm for 2000 steps using the CHARMM27 force field.[34] The resulting structure was immersed in water (10 Å TIP3 water model), and the charge was neutralized using 3 Na^+ ions. The particle-mesh Ewald method[35] and periodic boundary conditions were applied to complete the electrostatic calculations. We used Nose-Hoover Langevin piston pressure control and maintained the temperature at 310 K.[36] The SHAKE[37] method was used to provide an integration time step of 2 fs while keeping all bonds to the hydrogen atoms rigid. The equilibration protocol involved 1500 minimization steps followed by 30 ps of MD at 0 K for the water and ions while freezing the entire protein. Once the minimization of the entire system was achieved, the temperature was increased from 10 to 310 K over 30 ps to ensure that it would continue to modify its volume with 30 ps of NTP dynamics.[36] As a final step, the NTV dynamics continued for 20 ns. The trajectory of the system was stored every 1 ps, and the simulations were analyzed by capturing several snapshots every 1 ns. The snapshots, RMSD, RMSF, and Rg were obtained using the carma program[38] based on the following equations. The RMSD was analyzed to determine whether the protein had undergone a conformational change because this value reflects the distance between pairs of the same atoms represented by δ with respect to time. However, the RMSF indicates the displacement of the particle, as observed in Eq. (2). Therefore, the RMSF average is taken over time to give a value for each particle, whereas the RMSD average is calculated over the particles to provide time-specific values.

$$RMSD = \sqrt{\frac{1}{N}\sum_{i=1}^{N}\delta_i^2} \quad (1)$$

$$RMSF = \sqrt{\frac{1}{T}\sum_{t_j=1}^{T}\left(x_i(t_j)-\tilde{x}_i\right)^2} \quad (2)$$

All the computational work was performed using pmemd cuda on an Intel Core i7–980x 3.33 Ghz Linux workstation with 12 Gb of RAM, (2x) NVIDIA Geforce GTX530 video cards, and (1x) NVIDIA Geforce GTX580 video card.

MD simulations of $A\beta_{1-42}$ -Cu^{2+}. To perform MD simulations that included Cu^{2+}, the parameters of Cu^{2+} were added to the topology (MASS 63.54600, RESI CU2 2.00) and parameter (CU 0.000000–0.250000 1.090000 ION) files. The coordinates of Cu^{2+} were taken from the crystallized structure of cytochrome C oxidase (PDB code: 1OCO),[39] and 1 Cu^{2+} ion was placed near the Hys 6, 13, and 14 amino acid residues because these residues have been reported to be capable of binding Cu^{2+}. Hydrogen atoms were added with the psfgen command within the VMD program,[33] and the structures were minimized using the steepest descent algorithm for 2000 steps using the CHARMM27 force field. The structure was immersed in water (10 Å TIP3 water model), and the charge was neutralized using 1 Na^+ ions. The methodology for this MD simulation was similar to that described for $A\beta_{1-42}$ in the absence of Cu^{2+}.

Two MD simulations were performed. The first consisted of an evaluation of the conformational

change of $A\beta_{1-42}$ in the α-helix conformation in the presence of 1 Cu^{2+} ion. The second simulation was performed using $A\beta_{1-42}$ in the β-sheet conformation (reached by MD simulations using a snapshot retrieve at 13 ns) in the presence of 1 Cu^{2+} ion to assess the effect of Cu^{2+} in shaping the secondary structure of $A\beta_{1-42}$ using the procedure described above.

MD simulation of the binding of galanthamine to $A\beta_{1-42}$ in the α-helix conformation. The input galanthamine coordinates were taken from the structure with PDB code 1DX6[40] and placed near Hys 6, 13, and 14. Hydrogen atoms were added with the psfgen command within the VMD program,[33] and the structure was minimized using the steepest descent algorithm for 2000 steps using the CHARMM27 force field. The structure was immersed in water (10 Å TIP3 water model), and the charge was neutralized using 2 Na^+ ions. The parameters and topology for galanthamine were calculated using the online SwissParam server (http://www.swissparam.ch/). The methodology for the MD simulations was similar to that previously described.

MD simulation analyses. The analyses of the MD simulation results were performed using the carma software package.[38] The root-mean-square deviation (RMSD) of the alpha carbon (Cα) from the backbone residues, the root-mean-square fluctuation (RMSF) of the backbone residue atoms and the ratio of gyration (Rg) of Cα were determined. All the molecular graphical presentations from the docking and MD simulations were created using the PyMOL package (http://www.pymol.org/).

Docking method

A docking study was performed using two different Aβ monomers to construct their respective oligomers. The first monomer was the conformer obtained from the MD simulations at 20 ns using the Aβ PDB code 1Z0Q model 1, and the second was the Aβ obtained from the 2BEG structure. The docking was performed on a ClusPro2.0 server (http://cluspro.bu.edu).[19] To obtain an Aβ dimer (lowest free energy), two of the same monomers were used. The ClusPro2.0 server, one of the top performers at CAPRI (Critical Assessment of Predicted Interactions) round 13–19,[20] was used to predict the possible structure of the oligomers. We submitted to ClusPro two monomers to obtain the dimer, which was used to dock with another monomer to form a trimer, and so forth; this process was performed until an Aβ pentamer was formed.

ClusPro selects the 1000 best scoring solutions and then clusters them according to root mean square deviation (RMSD) considerations. Each cluster is characterized by its number of members, the ClusPro score of the center of the cluster and the lowest ClusPro score found in the cluster. We used the balance favored by hydrophobic interactions, VdW interactions and electrostatic interactions according to ClusPro score.[20]

Evaluation of $A\beta_{1-42}$ aggregation by thioflavin T fluorescence

Lyophilized wild-type human $A\beta_{1-42}$ peptide (chloride salt; Calbiochem) was purchased from Merck Mexico. HEPES sodium salt (>99.5% purity), ThT, $CuCl_2$, and galanthamine were obtained from Sigma-Aldrich (Mexico). All solutions were prepared in fresh Milli-Q water. A freshly prepared solution of $A\beta_{1-42}$ with a concentration of 62.9 μ*M* was incubated alone and in the presence of 20 μ*M* $CuCl_2$ [22] or 100 μ*M* galanthamine[13] because at these concentrations $A\beta_{1-42}$ oligomerization is inhibited. The samples were incubated at 37°C in a quartz cell for 24 h with a 0.5-cm path length, and were subsequently stirred at 250 rpm. The increase in ThT fluorescence was measured at 480 nm using 445-nm excitation on a Perkin Elmer LS-55 fluorescence spectrophotometer equipped with a water-jacketed cell holder for temperature control. All the experiments were performed at 37°C using quartz cells with a path length of 1.0 cm, 20 m*M* HEPES, 100 m*M* NaCl, a pH of 7.4, and a ThT concentration of 3.3 μ*M*, as described in a previous report.[22] To obtain the corresponding graphics, the results of the spectra for Cu^{2+} and galanthamine were subtracted from the spectra from ThT.

Circular Dichroism measurements

The lyophilized wild-type human $A\beta_{1-42}$ peptide was diluted in Milli-Q water to a final concentration of 50 μ*M*, as reported by Salomon.[41] The $A\beta_{1-42}$ solution was incubated at 37°C in the absence and presence of 20 μ*M* $CuCl_2$ or 100 μ*M* galanthamine. CD spectra were acquired using a JASCO J-815 spectropolarimeter (Jasco, Easton, MD) equipped with a PFD-425S Peltier-type cell holder for temperature control at 37°C and magnetic stirring. Three accumulations of the CD spectra were recorded from 200 to 250 nm using 1.0-mm path-length quartz cells. The data were collected each hour for 3 h of incubation. The data were corrected by subtracting the spectrum of a sample that contained all of the components except Aβ. The data were converted to mean residue ellipticity and analyzed using the CDPro software package.[42]

References

1. Fitten LJ, Ortiz F, Pontón M (2001) Frequency of Alzheimer's disease and other dementias in a community outreach sample of Hispanics. J Am Geriatr Soc 49: 1301–1308.
2. Gilbert BJ (2013) The role of amyloid β in the pathogenesis of Alzheimer's disease. J Clin Pathol 66: 362–366.
3. Conway KA, Baxter EW, Felsenstein KM, Reitz AB (2003) Emerging beta-amyloid therapies for the

treatment of Alzheimer's Disease. Curr Pharm Des 9: 427–447.
4. Weksler ME, Gouras G, Relkin NR, Sxabo P (2005) The immune system, amyloid β peptide and Alzheimer's disease. Immun Res 205:244–256.
5. Sciarretta KL, Gordon DJ, Petkova, AT, Tycko R, Meredith SC (2005) Aβ40-lactam (D23/K28) models a conformation highly favorable for nucleation of amyloid. Biochemistry 44:6003–6014.
6. Tougu V, Tiiman A, Palumaa P (2011) Interactions of Zn (II) and Cu (II) ions with Alzheimer's amyloid-betapeptide metal ion binding, contribution to fibrillization and toxicity. Metallomics 3:250–261.
7. Chen WT, Liao YH, Yu HM, Cheng IH, Chen YR (2011) Distinct effects of Zn^{2+}, Cu^{2+}, Fe^{3+}, and Al^{3+} on amyloid-β stability, oligomerization, and aggregation. J Biol Chem 286:9646–9656.
8. Zhu XB, Wang X, Smith MA, Perry G (2007) Causes of oxidative stress in Alzheimer disease. Cell Mol Life Sci 64:2202–2210.
9. Parthasarathy S, Long F, Miller Y, Xiao Y, McElheny D, Thurber K, Nussinov R, Ishii Y (2011) Molecular-level examination of Cu^{2+} binding structure for amyloid fibrils of 40-residue Alzheimer's β by solid-state NMR spectroscopy. J Am Chem Soc 133:3390–3400.
10. Gaeta A, Molina-Holgado F, Kong XL, Salvage S, Fakih S, Francis PT, Williams RJ, Hider RC (2011) Synthesis, physical–chemical characterisation and biological evaluation of novel 2-amido-3-hydroxypyridin-4(1H)-ones: iron chelators with the potential for treating Alzheimer's disease. Bioorg Med Chem 19: 1285–1297.
11. Merlini E, Ascari N, Amboldi N, Bellotti V, Arbustini E, Perfetti V, Ferrari M, Zorzoli I, Marinone M, Garini P, Diegoli M, Trizio D, Ballinari D (1995) Interaction of the anthracycline 4'-iodo-4'-deoxydoxorubicin with amyloid fibrils: inhibition of amyloidogenesis. Proc Natl Acad Sci USA 92:2959–2963.
12. Pappolla M, Bozner P, Soto C, Shao H, Robakis NK, Frangione B, Ghiso J (1998) Inhibition of Alzheimer's beta fibrillogenesis by melatonin. J Biol Chem 273: 7185–7188.
13. Matharu B, Gibson G, Parsons R, Huckerby TN, Moore SA, Cooper LJ, Millichamp R, Allsop D, Austen B (2009) Galantamine inhibits β-amyloid aggregation and cytotoxicity. J Neurol Sci 280:49–58.
14. Masman MF, Ulrich, LM, Csizmadia IG, Penke B, Enriz RD, Marrink SJ, Luiten P (2009) *In silico* study of full-length amyloid beta 1–42 tri- and penta-oligomers in solution. J Phys Chem B 113:11710–11719.
15. Lührs T, Ritter C, Adrian M, Riek-Loher D, Bohrmann B, Döbeli H, Schubert D, Riek R (2005) 3D structure of Alzheimer's amyloid-beta (1–42) fibrils. Proc Natl Acad Sci USA 102:17342–17347.
16. Liu, R, McAllister C, Luybchenko Y, Sierks MR (2004) Residues 17–20 and 30–35 of beta amyloid play critical roles in aggregation. J Neurosci Res 5:162–171.
17. Kozakov D, Hall DR, Beglov D, Brenke R, Comeau SR, Shen Y, Li K, Zheng J, Vakili P, Paschalidis IC, Vajda S (2010) Achieving reliability and high accuracy in automated protein docking: cluspro, PIPER, SDU, and stability analysis in CAPRI rounds 13–19. Proteins 78: 3124–3130.
18. Kozakov D, Brenke R, Comeau SR, Vajda S (2006) PIPER: an FFT-based protein docking program with pairwise potentials. Proteins 65:392–406.
19. Drew SC, Barnham KJ (2011) The heterogeneous nature of Cu^{2+} interactions with Alzheimer's amyloid-β peptide. Acc Chem Res 44:1146–1155.
20. Jun S, Gillespie JR, Shin BK, Saxena S (2009) The second Cu(II)-binding site in a proton-rich environment interferes with the aggregation of amyloid-β (1−40) into amyloid fibrils. Biochemistry 48:10724–10732.
21. Levine H (1993) Thioflavine T interaction with synthetic Alzheimer's disease beta-amyloid peptides: detection of amyloid aggregation in solution. Protein Sci 2: 404–410.
22. Tougu, V, Karafin A, Palumaa P (2008) Binding of zinc (II) and copper(II) to the full-length Alzheimer's amyloid-beta peptide. J Neurochem 110:1784–1795.
23. Chiti F, Dobson CM (2006) Protein misfolding, functional amyloid and human disease. Annu Rev Biochem 75:333–366.
24. Babic T (1999) The cholinergic hypothesis of Alzheimer's disease: a review of progress. J Neurol Neurosurg Psychiatry 67:558.
25. Raffa DF, Rauk A (2007) Molecular dynamics to study of the beta amyloid peptide of Alzheimer's disease and its divalent copper complexes. J Phys Chem B 111: 3789–3799.
26. Mantri, Y, Fioroni M, Baik M (2008) Computational study of the binding of CuII to Alzheimer's amyloid-b peptide: do Ab42 and Ab40 bind copper in identical fashion? J Biol Inorg Chem 13:1197–1204.
27. Furlan S, Hureau C, Faller P, La Penna G (2012) Modeling copper binding to the amyloid-β peptide at different pH: toward a molecular mechanism for Cu reduction. J Phys Chem B 116:11899–11910.
28. Rao PN, Mohamed T, Osman W (2013) Investigate the binding interactions of galantamina with β-amyloid peptide. Bioorg Med Chem Lett 23:239–243.
29. Miller Y, Ma B, Nussinov R (2010) Polymorphism in Alzheimer Aβ amyloid organization reflects conformational selection in a rugged energy landscape. Chem Rev 110:4820–4838.
30. Sreerama N, Woody R (2003) Structural composition of βI- and βII proteins. Protein Sci 12:384–388.
31. Tomaselli S, Esposito V, Vangone P, van Nuland NA, Bonvin AM, Guerrini R, Tancredi T, Temussi PA, Picone D (2006) The alpha-to-beta conformational transition of Alzheimer's A beta-(1–42) peptide in aqueous media is reversible: a step by step conformational analysis suggests the location of beta conformation seeding. ChemBioChem 7:257–267.
32. Kal'e L (1999) NAMD2: greater scalability for parallel molecular dynamics. J Comput Phys 151:283–312.
33. Humphrey W, Dalke A, Schulten K (1996) VMD: visual molecular dynamics. J Mol Graph 14:33–38.
34. Zhu X, Lopes PEM, MacKerell AD (2012) Recent developments and applications of the CHARMM force fields. WIREs 2:167–185.
35. Batcho PF, Case DA, Schlick T (2001) Optimized particle-mesh Ewald/multiple-timestep integration for molecular dynamics simulation. J Chem Phys 115: 4003–4041.
36. Martyna GJ, Tobias DJ, Klein ML (1994) Constant-pressure molecular-dynamics algorithms. J Chem Phys 101:4177–4189.
37. Ryckaert JP, Ciccotti G, Berendsen HJ (1977) Numerical integration of the cartesian equations of motion of a system with constrains. J Comput Phys 23:327–341.
38. Glykos NM (2006) Carma: a molecular dynamics analysis program. J Comput Chem 27:1765–1768.

39. Soulimane T, Than ME, Dewor M, Huber R, Buse G (2000) Primary structure of a novel subunit in ba3-cytochrome oxidase from Thermus thermophiles. Protein Sci 11:2068–2073.
40. Greenblatt HM, Kryger G, Lewis T, Silman I, Sussman JL (1999) Structure of acetylcholinesterase complexed with galantamine at 2.3 A resolution. FEBS Lett 17:321–326.
41. Salomon AR, Marcinowski KJ, Friedland RP, Zagorski MG (1996) Nicotine inhibits amyloid formation by the β-peptide. Biochemistry 35:13568–13578.
42. Chen H, Yang JT, Chau KH (1974) Determination of the helix and b-form of proteins in aqueous solution by circular dichroism. Biochemistry 13: 3350–3359.